Band Structures of Plasmonic Polarons

Fabio Caruso, Henry Lambert, and Feliciano Giustino

Department of Materials, University of Oxford, Parks Road, Oxford OX1 3PH, United Kingdom

Using state-of-the-art many-body calculations based on the "*GW* plus cumulant" approach, we show that electron-plasmon interactions lead to the emergence of plasmonic polaron bands in the band structures of common semiconductors. Using silicon and group IV transition-metal dichalcogenide monolayers (AX_2 with $A = $ Mo,W and $X = $ S, Se) as prototypical examples, we demonstrate that these new bands are a general feature of systems characterized by well-defined plasmon resonances. We find that the energy versus momentum dispersion relations of these plasmonic structures closely follow the standard valence bands, although they appear broadened and blueshifted by the plasmon energy. Based on our results, we identify general criteria for observing plasmonic polaron bands in the angle-resolved photoelectron spectra of solids.

Electron-boson interactions are pervasive in many-body physics, and the resulting quasiparticles are clear examples of emergent behavior in quantum matter. While in the case of phonons and magnons the fingerprints of their interactions with electrons in angle-resolved photoemission spectra (ARPES) are largely understood [1], much less is known about electron-plasmon interactions. A detailed and quantitative description of these interactions is key to refine our understanding of electronic excitations in condensed matter and could provide new pathways towards plasmon-assisted band-gap tuning [2], or the manipulation of plasmon polaritons, with potential implications for photonics and plasmonics [3].

In ARPES, the acceleration of a photo-electron upon photon absorption may trigger shake-up excitations in the sample, leading to the emission of phonons, electron-hole pairs, and plasmons, the latter being collective charge-density fluctuations [4]. Intuitively, if a photon excites both a hole and a plasmon, the ARPES signal should exhibit spectral weight at energies corresponding to the sum of the binding energy of the electron and the excitation energy of the plasmon, as obtained, for example, by electron energy loss spectroscopy (EELS) [5]. This phenomenology is analogous to the emergence of "peak-dip-hump" structures in ARPES as a result of electron-phonon interactions [1,6–11]; the difference between the resulting spectral features arises from the characteristic energy of the boson (∼10 meV for phonons, ∼10 eV for plasmons). In fact, the very first model of electron-plasmon interactions [4,12,13] is formally equivalent to the electron-phonon Hamiltonian developed for the polaron problem [14]. In this model, the electron-plasmon interaction results in "plasmonic polarons" [15], in complete analogy with the polarons of the ordinary theory of electron-phonon interactions [16].

Identifying plasmonic polarons in ARPES spectra is notoriously difficult. While plasmonic satellites have been successfully identified in the *integrated* photoemission spectra of Na [17] and Si [18], the identification of energy versus momentum dispersions of plasmonic polarons in *angle-resolved* spectra has proven considerably more challenging [19]. So far, such dispersions have been observed only in the case of graphene and only in a narrow region of the Brillouin zone around the Dirac point [20,21]. Key factors hindering the observation of the dispersion relations of plasmonic polarons are (i) the energy scale of the plasmon energy, which requires using energetic photons at the expense of momentum resolution, (ii) the increased phase space for electron-phonon scattering and electron-hole pair generation, which adds to the spectral broadening, and (iii) the possible mixup of weak plasmonic satellites and strong quasiparticle peaks.

In this work, we perform state-of-the-art first-principles calculations to show that electron-plasmon interactions lead to the formation of plasmonic-polaron band-structure replica. These new structures appear as broadened copies of the valence bands shifted by the plasmon energy. Using a combination of many-body perturbation theory in the *GW* approximation [22–24] and the cumulant expansion approach [4,13,17,18,25–29], we demonstrate the presence of plasmonic-polaron bands in silicon. We further show that two-dimensional group IV transition-metal dichalcogenides (TMDs) AX_2 with $A = $ Mo, W and $X = $ S, Se [30,31] provide an ideal playground for the experimental observation of these novel spectroscopic signatures of the electron-plasmon coupling.

Within the sudden approximation, the photocurrent measured in ARPES experiments is proportional to the electron spectral function $A(\mathbf{k}, \omega)$ [1,32], where $\mathbf{k}$ is the crystal momentum of the electron and ω its binding energy (here and in the following, atomic units are understood). The spectral function can be calculated by using the cumulant expansion [4,13,17,18,26]: The electron Green's function is expanded in terms of the screened Coulomb interaction W, and a subset of diagrams is evaluated to all orders of perturbation [4]. This

strategy leads to a more accurate treatment of dynamical correlation as compared to the standard GW approximation [22]. The cumulant expansion draws from the exact solution of the polaron problem [16] and was originally applied to study plasmon satellites in core-level spectra [13]. Importantly, it is also valid in the case of valence electrons, as the effects of electron recoil (change of electron momentum) upon plasmon emission tend to cancel out [4].

In this work, we use the formulation of the cumulant expansion given by [4] and [17], which we will refer to as the $GW + C_{AHK}$ approach. In this formulation, only the first cumulant is retained in order to describe the line shape of quasiparticles and one-plasmon excitations. The case of n-plasmon excitations ($n \geq 2$) is of little interest here since the corresponding spectral signatures are damped by the Lang-Firsov factor $a^n/n!$, with a the average number of plasmons around the hole [13]. The $GW + C_{AHK}$ spectral function can be expressed as [17]

$$A(\mathbf{k}, \omega) = \sum_n [A_n^{QP}(\mathbf{k}, \omega) + A_n^{QP}(\mathbf{k}, \omega)A_n^C(\mathbf{k}, \omega)]. \quad (1)$$

Here A_n^{QP} denotes the quasiparticle contribution to the G_0W_0 spectral function:

$$A_n^{QP}(\mathbf{k}, \omega) = \frac{1}{\pi} \frac{|\Sigma''_{n\mathbf{k}}(\varepsilon_{n\mathbf{k}})|}{[\omega - \varepsilon_{n\mathbf{k}} - \Sigma'_{n\mathbf{k}}(\varepsilon_{n\mathbf{k}})]^2 + [\Sigma''_{n\mathbf{k}}(\varepsilon_{n\mathbf{k}})]^2}, \quad (2)$$

where Σ' (Σ'') indicates the real (imaginary) part of the G_0W_0 self-energy [22,23], and $\varepsilon_{n\mathbf{k}}$ the Kohn-Sham eigenvalue. In Eq. (2), it is assumed that the off-diagonal elements of the self-energy are small and can be neglected, as is typically the case [23,33]. The term A_n^C in Eq. (1) is defined as [17]

$$A_n^C(\mathbf{k}, \omega) = \frac{\beta_{n\mathbf{k}}(\omega) - \beta_{n\mathbf{k}}(\varepsilon_{n\mathbf{k}}) - (\omega - \varepsilon_{n\mathbf{k}})\frac{\partial \beta_{n\mathbf{k}}}{\partial \omega}\big|_{\varepsilon_{n\mathbf{k}}}}{(\omega - \varepsilon_{n\mathbf{k}})^2}, \quad (3)$$

where $\beta_{n\mathbf{k}}(\omega) = \pi^{-1}\Sigma''_{n\mathbf{k}}(\omega)\theta(\mu - \omega)$, μ being the chemical potential. This term accounts for interactions between the photo-hole and one-plasmon excitations [32], and its contribution to the spectral function in Eq. (2) is to be identified with plasmonic polarons.

Using Eqs. (1)–(3), we now investigate the signatures of plasmonic polarons in silicon. In Figs. 1(a) and 1(b), we report the angle-resolved spectral function of silicon obtained from the Sternheimer-G_0W_0 approach (SGW) and SGW plus cumulant (S$GW + C_{AHK}$), respectively. Details on SGW are provided in Refs. [34,39,40]. For silicon, the experimental (integrated) photoemission spectrum shown in Fig. 1(c) is characterized by a broadened plasmonic resonance covering approximately the energy range from 16 eV to 30 eV below the Fermi energy. In this resonance, we can clearly identify three distinct structures (dashed blue lines). The bright energy bands visible in Fig. 1(a) for binding energies between 0 and 12 eV correspond to the standard quasiparticle peaks. These peaks
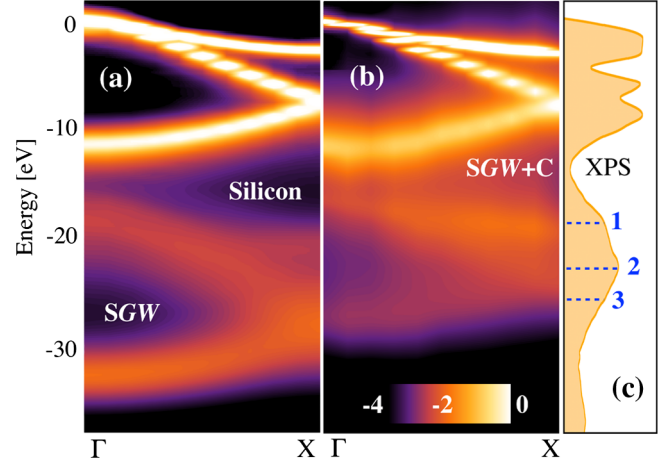

FIG. 1 (color online). Angle-resolved spectral function of silicon on a logarithmic scale for wave vectors along the Γ-X high-symmetry line, evaluated using (a) the Sternheimer-GW method (SGW) and (b) the SGW plus cumulant (S$GW + C_{AHK}$) approach. (c) Measured x-ray photoemission spectrum of silicon (XPS) from Ref. [18]. The blue dashed lines indicate the three features discussed in the main text.

result from photoionization processes occurring in the absence of plasmon excitations, and they define the ordinary valence band structure of silicon. In addition to the quasiparticle features, the spectral function exhibits a rich structure at binding energies between 15 and 30 eV. These structures can be identified with plasmonic polarons. These features are present already at the G_0W_0 level; however, their energy range is largely overestimated and, thus, not compatible with the plasmonic features observed in XPS. The inclusion of the cumulant correction in S$GW + C_{AHK}$ moves the plasmonic polaron resonances to lower binding energies, improving the agreement with the experimental spectrum significantly. This improvement reflects the inclusion of higher-order exchange-correlation diagrams in the $GW + C_{AHK}$ Green function, as discussed in more detail in Ref. [34].

Unexpectedly, plasmonic polarons exhibit dispersion relations which follow closely the ordinary band structure resulting from the quasiparticle peaks. The striking similarity between the dispersion of the valence bands and the plasmonic structures suggests that we are looking at *band structures* of plasmonic polarons. Plasmonic polaron bands appear as blueshifted replicas of the ordinary valence bands, but they are considerably broader and less intense. The comparison of Figs. 1(b) and 1(c) suggests that the plasmon satellite of silicon [18] results from the momentum average of plasmonic polaron bands over the first Brillouin zone. For quasiparticles, it is well known that the density of states is characterized by singularities (known as van Hove singularities) at the energies for which the first momentum derivative of the quasiparticle bands vanishes ($\nabla_{\mathbf{k}}\varepsilon_{\mathbf{k}} = 0$). Correspondingly, peaks in the density of states can be associated with extremal points of quasiparticle bands.
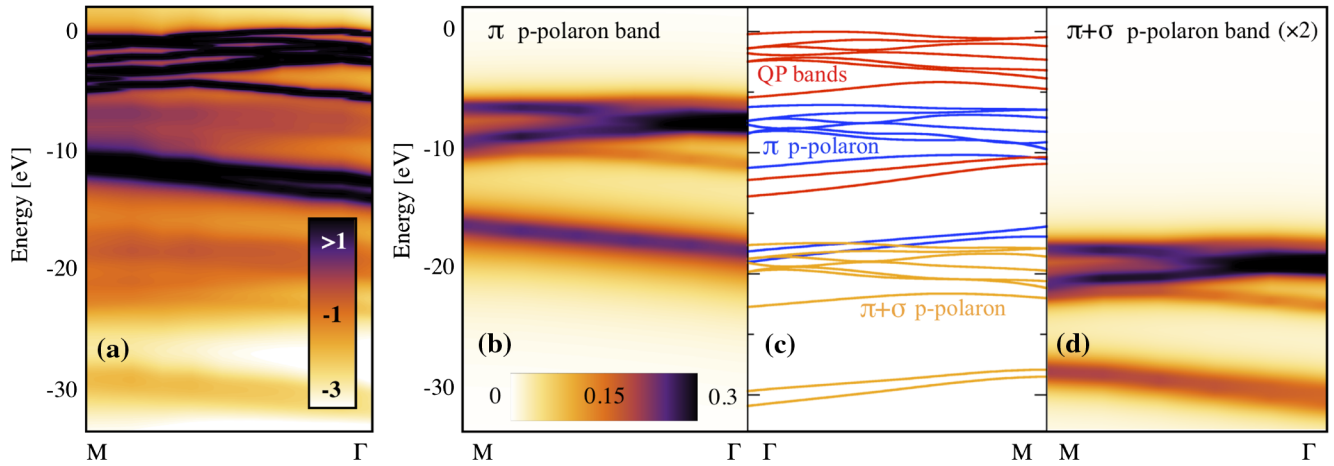
FIG. 2 (color online).   (a) Complete angle-resolved spectral function of monolayer MoS_2 on a logarithmic scale for wave vectors along the Γ-M high-symmetry line, evaluated using the $GW + C_{AHK}$ approach. (b,d) Contributions of plasmonic polarons to the spectral function in (a): π-plasmonic polarons (b) and $(\pi + \sigma)$-plasmonic polarons (d). (c) Quasiparticle band structure of monolayer MoS_2 extracted from (a) (red solid lines), band structure of π-plasmonic polarons extracted from (b) (blue solid line), and band structure of $(\pi + \sigma)$-plasmonic polarons from (d) (yellow solid line). Energies are referenced to the valence band top.

Figures 1(b) and 1(c) indicate that van Hove singularities may also have a plasmonic origin. In particular, the two experimental peaks at 20.4 eV and 24.5 eV and the shoulder at 27.3 eV [labeled as 1–3 in Fig. 1(c)] can be attributed to the vanishing of the first momentum derivative of the plasmonic polaron bands in Fig. 1(b).

Owing to the large plasmon energy, the experimental observation of plasmonic polaron bands in silicon may be hindered by the low resolution of ARPES measurements well below the Fermi energy. In order to identify materials in which such polaron bands may be observed, in the following we focus on group IV transition-metal dichalcogenides (MoS_2, WS_2, $MoSe_2$, and WSe_2). The EELS spectra of the three-dimensional parent compounds exhibit two distinct features around 8 eV and 22 eV, corresponding to the excitation of π and $\pi + \sigma$ plasmons, respectively [41,42]. Since the width of the bands arising from transition-metal d states and chalcogen p states in these compounds is approximately 7 eV [43], possible plasmonic polarons are expected to appear between 8 and 15 eV. In this energy range, the deep S-3s or Se-4s bands, located between 12 and 15 eV [43], dominate the spectral function, thereby also hindering the identification of plasmonic polarons in ARPES in this case.

At variance with this scenario, in the case of monolayer TMDs, both experimental [44] and theoretical [45] studies reported plasmonic peaks in the EELS spectra which are strongly redshifted with respect to their bulk counterpart. For example, in the case of MoS_2 and WS_2 monolayers, the π plasmons are found at energies around 6 eV. We thus expect to observe plasmonic polarons at binding energies between 6 and 13 eV. Since this energy window matches the band structure *gap* between the metal-d/chalcogen-p bands and the chalcogen s bands, such plamonic polarons should be distinctly observable.

To examine this possibility on quantitative grounds, we calculate the $GW + C_{AHK}$ spectral functions of TMDs from first principles [46]. In order to contain the computational cost, we describe the screening by introducing a two-pole approximation for the inverse dielectric matrix, as discussed in Ref. [34].

Figure 2(a) shows the complete $GW + C_{AHK}$ spectral function of monolayer MoS_2 evaluated along the Γ-M high-symmetry line. At binding energies between 0-5 eV and 10-15 eV, the spectral function of monolayer MoS_2 exhibits the standard quasiparticle peaks. As in the case of silicon, in monolayer MoS_2 plasmonic polarons introduce *new* spectral features in a binding energy range where quasiparticle states are absent. To characterize these new features, we analyze their energy versus wave vector dispersions using a Lorentzian decomposition of the energy profiles. This analysis allows us to disentangle the contributions of plasmonic polarons from the quasiparticle excitations. Figures 2(b) and 2(d) show the plasmonic polarons corresponding to the emission of a photoelectron and the simultaneous excitation of a π or $\pi + \sigma$ plasmon, respectively. As for silicon, plasmonic polarons exhibit a clear energy-momentum dispersion relation that leads to the formation of blueshifted replica of the valence band structure. In particular, we find two replicas of the valence bands of monolayer MoS_2, one associated with the π plasmon centered around the binding energy $\sim$8 eV, and another one associated with the $\pi + \sigma$ plasmon around 19 eV.

Owing to the approximate treatment of electron recoil effects in the cumulant approach [4,18], the actual broadening might be even larger than in the present calculations. In order to understand whether plasmonic polaron bands could be observed in ARPES experiments, it is therefore essential to quantify their spectral weight. A reliable measure of the intensity of the plasmonic bands can be
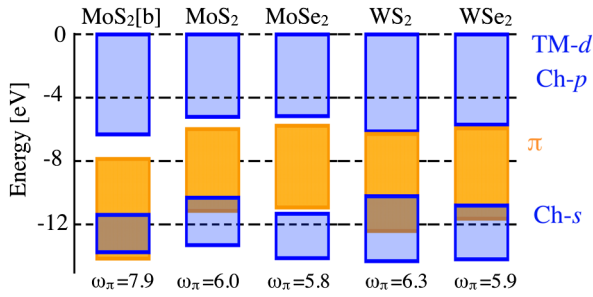
FIG. 3 (color online). Energy range of the quasiparticle bands (blue boxes) and the π-plasmonic polaron bands in monolayer MoS_2, $MoSe_2$, WS_2, and WSe_2, evaluated within the $GW + C_{AHK}$ approach (yellow boxes). Bulk MoS_2 is included for comparison ($MoS_2[b]$). The topmost bands arise from the hybridization of transition-metal d states and the chalcogenide p states (TM-d/Ch-p); the low-energy ones arise from the chalcogenide s states (Ch-s). The plasma energies ω_π are given in eV.

obtained from the average number $a_{n\mathbf{k}}$ of plasmons emitted during the photoemission process [32]: $a_{n\mathbf{k}} = \int \omega^{-2} \beta_{n\mathbf{k}}(\omega) d\omega$. In the case of the high-lying Mo-$4d$/S-$3p$ bands, we obtain $a_{n\mathbf{k}}$ in the range 0.08–0.12 for momenta along the Γ-M line, whereas $a_{n\mathbf{k}}$ is found in the range 0.04–0.06 for the lower-lying S-$3s$ bands. These results indicate that the formation of plasmonic polarons provides an important dissipation channel for the ARPES photocurrent. In particular, in the case of Mo-$4d_{z^2}$ states at the top of the valence band (the most important for electron transport in p-doped MoS_2), every photo-hole is accompanied by 0.13 plasmons. These estimates are confirmed by a direct integration of the spectral function, which shows that plasmonic polarons carry, on average, 12% of the total spectral weight of the valence electronic states. For the valence states, the intensity ratio between the plasmonic polaron band and the quasiparticle peak is ~0.01–0.02. In addition, by considering the metal-d/chalcogen-p bands together, we find that, in the case of monolayer MoS_2, it should be possible to extract up to 1.2×10^{14} electrons/cm^2 (0.1 electrons/cell) at binding energies inside the band structure gap between Mo-$4d$/S-$3p$ bands and S-$3s$ bands.

At variance with the case of monolayer MoS_2, for the bulk compound our calculations indicate that the plasmonic bands overlap substantially with the deep S-s states (Fig. 3). The overlap between ordinary quasiparticle bands and plasmonic polaron bands should make the experimental detection of these new features in bulk MoS_2 much more challenging than in the case of a monolayer.

The above results suggest that two key conditions need to be satisfied for plasmonic polaron band structures to be clearly observed in ARPES: (i) the existence of low-energy plasmon excitations in the EELS spectrum and (ii) the presence of a band gap in the valence band manifold. Condition (ii) also contributes to minimizing spectral broadening arising from electron-phonon scattering.

Given these "design rules," it is natural to ask whether there exist "optimal" TMDs for observing plasmonic polaron bands. To answer this question, we repeated our $GW + C_{AHK}$ calculations for the related monolayer compounds $MoSe_2$, WS_2, and WSe_2. Figure 3 shows that plasmonic polaron bands associated with π plasmons fit inside the band gap between the metal-d/chalcogen-p bands and the chalcogen-s bands for all these compounds. In particular, we find that monolayer $MoSe_2$ should provide an ideal test bench for identifying plasmonic polarons since, in this case, the plasmonic structures exhibit essentially no overlap with the ordinary valence bands (Fig. 3).

Since the plasmon energy scales with the square root of the static dielectric constant ϵ_0, it should also be possible to realize plasmonic band structure engineering in TMD monolayers by modifying their dielectric screening properties. For example, this could be achieved by using different substrates, by building van der Waals heterostructures of TMDs [51], or by using doping [52] or mechanical deformation [53,54]. All these modifications would leave the ordinary valence band structure essentially unaffected (on the eV scale) while producing significant shifts in the binding energy of plasmonic polarons.

In conclusion, using state-of-the-art first-principles GW plus cumulant calculations, we have shown that electron-plasmon coupling leads to the formation of plasmonic polaron band structures and that group IV transition-metal dichalcogenide monolayers (in particular, monolayer $MoSe_2$) should provide a unique opportunity for observing these new features in ARPES experiments. Remarkably, we have found that these plasmonic band structures exhibit dispersion relations which closely follow the ordinary valence bands and, similarly to quasiparticle bands, lead to the formation of van Hove singularities in the density of states. More generally, plasmonic-polaron bands emerge as novel spectroscopic signatures of electron-plasmon coupling, which may contribute to unravel the complexity of ARPES measurements. The emergence of plasmonic polarons is not limited to semiconductors and may also prove useful to rationalize the electronic structure of materials characterized by well-defined plasmonic excitations, including, for example, metals, as well as d- and f-electron systems [55,56]. In fact, our work raises the question of whether the concept of plasmonic polarons may be systematically employed in the interpretation of ARPES spectra of complex systems. As an example, while our work focused on the simplest case of "isolated" plasmonic polaron bands, the crossing of plasmonic bands and high-lying valence bands may reveal the emergence of band-branching effects, in analogy with the polaron problem in electron-phonon physics [57].

[1] A. Damascelli, Z. Hussain, and Z.-X. Shen, Rev. Mod. Phys. **75**, 473 (2003).

[2] Y. Liang and L. Yang, Phys. Rev. Lett. **114**, 063001 (2015).

[3] S. A. Maier and H. A. Atwater, J. Appl. Phys. **98**, 011101 (2005).

[4] L. Hedin, Phys. Scr. **21**, 477 (1980).

[5] P. Nozières and D. Pines, Phys. Rev. **113**, 1254 (1959).

[6] A. Lanzara et al., Nature (London) **412**, 510 (2001).

[7] A. Bostwick, T. Ohta, T. Seyller, K. Horn, and E. Rotenberg, Nat. Phys. **3**, 36 (2007).

[8] F. Giustino, M. L. Cohen, and S. G. Louie, Nature (London) **452**, 975 (2008).

[9] T. Dahm, V. Hinkov, S. V. Borisenko, A. A. Kordyuk, V. B. Zabolotnyy, J. Fink, B. Büchner, D. J. Scalapino, W. Hanke, and B. Keimer, Nat. Phys. **5**, 217 (2009).

[10] S. Moser et al., Phys. Rev. Lett. **110**, 196403 (2013).

[11] J. P. Carbotte, T. Timusk, and J. Hwang, Rep. Prog. Phys. **74**, 066501 (2011).

[12] B. I. Lundqvist, Phys. Kondens. Mater. **6**, 193 (1967).

[13] D. C. Langreth, Phys. Rev. B **1**, 471 (1970).

[14] S. Engelsberg and J. R. Schrieffer, Phys. Rev. **131**, 993 (1963).

[15] We purposely avoid the term "plasmarons" introduced by Lundqvist [12]. In the original formulation, the plasmaron was understood as a new elementary excitation resulting from a pole of the electron's Green's function. Subsequent analysis by Langreth [13] showed that the poles identified in [12] are an artifact of the *GW* approximation, but there exists a polaron resonance in analogy with the standard electron-phonon theory [4,13].

[16] G. Mahan, *Many-Particle Physics* (Springer, Berlin, 2000).

[17] F. Aryasetiawan, L. Hedin, and K. Karlsson, Phys. Rev. Lett. **77**, 2268 (1996).

[18] M. Guzzo, G. Lani, F. Sottile, P. Romaniello, M. Gatti, J. J. Kas, J. J. Rehr, M. G. Silly, F. Sirotti, and L. Reining, Phys. Rev. Lett. **107**, 166401 (2011).

[19] A. S. Kheifets, V. Sashin, M. Vos, E. Weigold, and F. Aryasetiawan, Phys. Rev. B **68**, 233205 (2003).

[20] A. Bostwick, F. Speck, T. Seyller, K. Horn, M. Polini, R. Asgari, A. H. MacDonald, and E. Rotenberg, Science **328**, 999 (2010).

[21] M. Polini, R. Asgari, G. Borghi, Y. Barlas, T. Pereg-Barnea, and A. MacDonald, Phys. Rev. B **77**, 081411 (2008).

[22] L. Hedin, Phys. Rev. **139**, A796 (1965).

[23] M. S. Hybertsen and S. G. Louie, Phys. Rev. B **34**, 5390 (1986).

[24] G. Onida, L. Reining, and A. Rubio, Rev. Mod. Phys. **74**, 601 (2002).

[25] B. Holm and F. Aryasetiawan, Phys. Rev. B **56**, 12825 (1997).

[26] J. Lischner, D. Vigil-Fowler, and S. G. Louie, Phys. Rev. Lett. **110**, 146801 (2013).

[27] M. Guzzo, J. J. Kas, F. Sottile, M. G. Silly, F. Sirotti, J. J. Rehr, and L. Reining, Eur. Phys. J. B **85**, 324 (2012).

[28] J. J. Kas, J. J. Rehr, and L. Reining, Phys. Rev. B **90**, 085112 (2014).

[29] M. Guzzo, J. J. Kas, L. Sponza, C. Giorgetti, F. Sottile, D. Pierucci, M. G. Silly, F. Sirotti, J. J. Rehr, and L. Reining, Phys. Rev. B **89**, 085425 (2014).

[30] B. Radisavljevic, A. Radenovic, J. Brivio, V. Giacometti, and A. Kis, Nat. Nanotechnol. **6**, 147 (2011).

[31] Q. H. Wang, K. Kalantar-Zadeh, A. Kis, J. N. Coleman, and M. S. Strano, Nat. Nanotechnol. **7**, 699 (2012).

[32] L. Hedin, J. Phys. Condens. Matter **11**, R489 (1999).

[33] F. Bruneval, N. Vast, and L. Reining, Phys. Rev. B **74**, 045102 (2006).

[34] See Supplemental Material at http://link.aps.org/supplemental/10.1103/PhysRevLett.114.146404, for details on the theoretical methods, which includes Refs. [35–38].

[35] R. W. Godby and R. J. Needs, Phys. Rev. Lett. **62**, 1169 (1989).

[36] G. E. Engel and B. Farid, Phys. Rev. B **47**, 15931 (1993).

[37] S. Baroni, S. de Gironcoli, and A. Dal Corso, Rev. Mod. Phys. **73**, 515 (2001).

[38] A. Frommer, Computing **70**, 87 (2003).

[39] F. Giustino, M. L. Cohen, and S. G. Louie, Phys. Rev. B **81**, 115105 (2010).

[40] H. Lambert and F. Giustino, Phys. Rev. B **88**, 075117 (2013).

[41] W. Y. Liang and S. L. Cundy, Philos. Mag. **19**, 1031 (1969).

[42] M. Bell and W. Liang, Adv. Phys. **25**, 53 (1976).

[43] P. Raybaud, J. Hafner, G. Kresse, and H. Toulhoat, J. Phys. Condens. Matter **9**, 11107 (1997).

[44] J. N. Coleman et al., Science **331**, 568 (2011).

[45] P. Johari and V. B. Shenoy, ACS Nano **5**, 5903 (2011).

[46] Ground-state density-functional theory calculations in the local density approximation (LDA) [47,48] are performed using the Quantum-ESPRESSO software package [49]. We used norm-conserving Hartwigsen-Goedeker-Hutter pseudopotentials and a 29 Ry kinetic energy cutoff, which suffices for converging the quasiparticle energies of MoS_2 [50]. The Brillouin zone is sampled using a 20×20 Monkhorst-Pack grid. For monolayer MoS_2, we employed a supercell approach with a 16.4 Å interlayer spacing between periodic replicas. In the $GW + C_{AHK}$ spectral function [Eqs. (1)–(3)], we neglect the asymmetry factor [4] and the exchange part of the quasiparticle correction as we are primarily interested in the intensity and binding energy of the spectral features. Sternheimer-GW calculations for silicon employ the same computational parameters as in [40].

[47] W. Kohn and L. J. Sham, Phys. Rev. **140**, A1133 (1965).

[48] P. Hohenberg and W. Kohn, Phys. Rev. **136**, B864 (1964).

[49] P. Giannozzi et al., J. Phys. Condens. Matter **21**, 395502 (2009).

[50] F. Hüser, T. Olsen, and K. S. Thygesen, Phys. Rev. B **88**, 245309 (2013).

[51] A. K. Geim and I. V. Grigorieva, Nature (London) **499**, 419 (2013).

[52] B. Radisavljevic and A. Kis, Nat. Mater. **12**, 815 (2013).

[53] A. Castellanos-Gomez, R. Roldán, E. Cappelluti, M. Buscema, F. Guinea, H. S. J. van der Zant, and G. A. Steele, Nano Lett. **13**, 5361 (2013).

[54] H. Peelaers and C. G. Van de Walle, Phys. Rev. B **86**, 241401 (2012).

[55] M. Gatti and M. Guzzo, Phys. Rev. B **87**, 155147 (2013).

[56] S. Basak, T. Das, H. Lin, J. Nieminen, M. Lindroos, R. S. Markiewicz, and A. Bansil, Phys. Rev. B **80**, 214520 (2009).

[57] A. Eiguren, C. Ambrosch-Draxl, and P. M. Echenique, Phys. Rev. B **79**, 245103 (2009).